Photonic Lanterns as Wavefront Sensors

Sergio G. Leon-Saval
Sydney Astrophotonic Instrumentation Laboratory, School of Physics, The University of Sydney, NSW 2006, Australia
Institute of Photonics and Optical Science, School of Physics, The University of Sydney, NSW 2006, Australia
Sergio.Leon-Saval@sydney.edu.au

Abstract: Photonic lanterns are low-loss mode convertors easily integrated with optical fiber technologies. We present the proof of concept of a focal plane low-order wavefront sensor based on a 19-core multicore photonic lantern and deep learning.

OCIS codes: (060.2280) Fiber design and fabrication; (060.2340) Fiber optics components; (010.1080) Active or adaptive optics.

1. Introduction

Adaptive optics (AO) is critical in astronomy, optical communications, remote sensing, and optical beam manipulation to correct distortions caused by propagation through media like the Earth's atmosphere or living tissue. But current AO systems are limited by their wavefront sensors, which need to be in an optical plane non-common to the science image and are insensitive to certain wavefront-error modes. A wavefront sensor that can be placed at the same focal plane as the science image and is optimal for single-mode fiber injection is highly desirable.

A relatively new waveguide technology that, by its intrinsic working mechanism, can give significant information of the light intensity and phase at its input based on its optical transmission is the photonic lantern [1,2]. This technology forms a low-loss interface between a multimode waveguide and a set of few-mode and/or single-mode waveguides. Most generally, it consists of an array of single-mode (SM) waveguides that are interfaced to a multimode (MM) waveguide through a physical waveguide transition. By matching the number of modes in this system, i.e. degrees of freedom, lossless coupling becomes possible by conserving the entropy of the system; this is a necessary but not sufficient condition. In the case of a MM to SM transition the final intensities and phases of the SM outputs will have a direct relationship to both phase and amplitude information of the incident wavefront.

2. Photonic lanterns as focal-plane wavefront sensors

In AO, a wavefront analyzer is employed to determine the degree and type of aberration in the beam, while the optical wavefront is altered and corrected employing a reconfigurable optical element. A new type of intensity-based fiber wavefront sensors based on a photonic lantern fiber-mode-converters with deep learning and/or direct intensity mapping from the input phase and intensity have been proposed and demonstrated [18,19]. In previous efforts a photonic lantern-like structure was simulated to measure the tip and tilt of an injected beam [23], but now higher order terms describing the shape of the wavefront could be measured. These bespoke photonic lantern wavefront sensors (PL-WFS) can be placed at the same focal plane as the science image and are optimal for SM fiber injection. In the PL-WFS, light is injected directly into the multimode region of a photonic lantern. The photonic lantern then converts the multiple modes in the MM fiber and into an array of uncoupled SM outputs, with the distribution of flux between the outputs determined by the corresponding power in each mode at the input. Hence both phase and amplitude information on the incident wavefront can be reconstructed.

3. Numerical simulation and theory

Since the modes excited within a MM fiber are a function of the electric field at the input, by measuring the relative power in each mode at the fiber's output it is in principle possible to reconstruct spatial information describing the input beam. Although power mixes between the various modes of the fiber as it propagates, as long as the fiber remains unperturbed (e.g. by strain or temperature) then the relationship between the input and output mode fields can be determined. Crucially, the monolithic nature of the photonic lantern device where the mode conversion occurs (typically 20-60mm in length) means that, once manufactured, the relationship between the modes excited in the multimode region and the distribution of light in the uncoupled single-mode outputs is deterministic and unchanging. Once in the form of SM cores, the information is robust – it is encoded in only the intensity of each core, which is essentially unaffected by small perturbations.

Although a simple intensity image of the point spread function (PSF) does not contain the necessary information to reconstruct the wavefront, the combination of modes excited within a MM fiber is a function of both the phase and the amplitude of the incoming light. Hence if the power in each mode of the fiber is known, it should be possible to infer the complex wavefront of an injected PSF. To validate the approach, a series of simulations were performed. First, a wavefront containing Zernike aberrations is produced and the complex electric field of the resulting PSF is obtained. This is then input into a model of the photonic lantern built using the RSoft software from Synopsis. Here, a numerical simulation is performed wherein the electric field is allowed to propagate from the multimode end to the single-mode outputs.

The result of one simulation demonstrating this concept is shown in Figure 1(b), wherein the phase of the wavefront, the intensity and phase of the resulting PSF after focusing and adding astigmatism, and the intensity of the 19 single-mode core outputs of the photonic lantern are given. The results for five wavefronts are shown – one with a flat wavefront, two with +0.8 radians and -0.8 radians of astigmatism respectively, and the other two with +2.0 radians and -2.0 radians of focus respectively. It is important to note that, in these cases, the intensity structure of the PSFs are identical for the two pairs of aberrated PSFs, and so a conventional imaging sensor at the focal plane would not be able to distinguish them. However, the necessary information is contained within the phase structure of the PSF, which is successfully measured by the photonic lantern and encoded in the intensity of its outputs giving very distinct solutions.

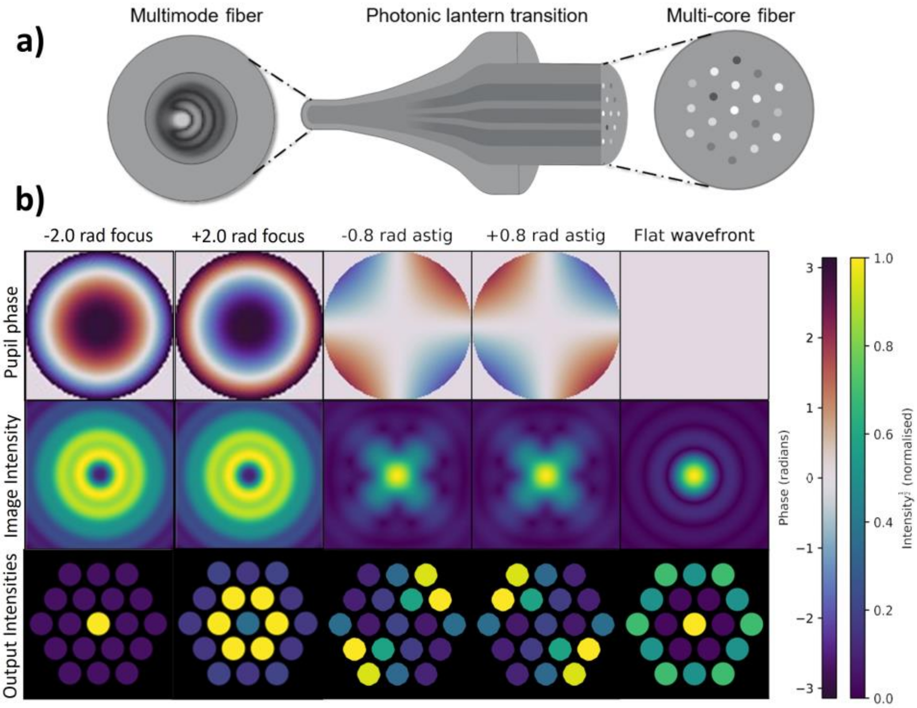

Fig.1. (a) Schematics of the 19-core multicore PL-WFS. (b) Typical intensity output of the multicore photonic lantern outputs versus the input image plane phase, demonstrating the concept of the photonic lantern wavefront sensor, and its ability to measure both amplitude and phase. The first row shows the pupil phase of the wavefront, and the second row shows the intensity of the resulting PSF respectively. The third row shows the intensities of the 19 single-mode outputs of the photonic lantern, when the corresponding PSF is injected.

These numerical simulations also demonstrated the non-linear response of the lantern's output intensities to wavefront phase. A series of simulations were run where a defocus term of changing amplitude is applied, and the output intensities of the lantern plotted as a function of defocus amplitude. It was seen that the 19 output intensities are not a linear function of phase, suggesting that using a linear algorithm (such as used conventionally in adaptive optics) to reconstruct the input phase would perform poorly. Hence, since the relationships between input phase and output intensities is non-linear, a deep neural network can be used to perform the reconstruction. These deep learning methods [24] have recently exploded in popularity across many fields of science and engineering. In essence, a neural network learns the relationship between the inputs (in this case wavefront phase) and outputs (in this case the intensities of the single-mode core lantern outputs) of some system. Then, given a new, previously unseen set of outputs, it can infer what the input is.

4. Results: laboratory demonstration

To validate the ability of the PL-WFS to determine the wave-front phase from the focal plane, a laboratory experiment was performed and the ability to recover the incident wavefront errors from the PL outputs was demonstrated. The experimental testbed provided the ability to inject a PSF arising from an arbitrary wavefront (created using a spatial-light modulator (SLM)) into a 19-core multicore photonic lantern and measure the 19 output intensities. The PL used here was made using a multicore fiber with 19 uncoupled 3.7 µm cores, NA of 0.14, and core-to-core separation of

35μm that is tapered with a low-index glass capillary (fluorine doped fused silica) jacket to produce a 22 μm MM input with an NA of 0.145. The experimental layout is shown in Figure 3. For each laboratory measurement, a combination of the first 9 (non-piston) Zernike terms were simultaneously applied to the SLM, each with an amplitude randomly chosen between approximately -0.12π and 0.12π radians. After these aberrations are combined the resulting phase error for each measurement has a peak-to-valley amplitude of approximately π radians. This was a limit imposed by the maximum retardance the SLM can produce within its linear range.

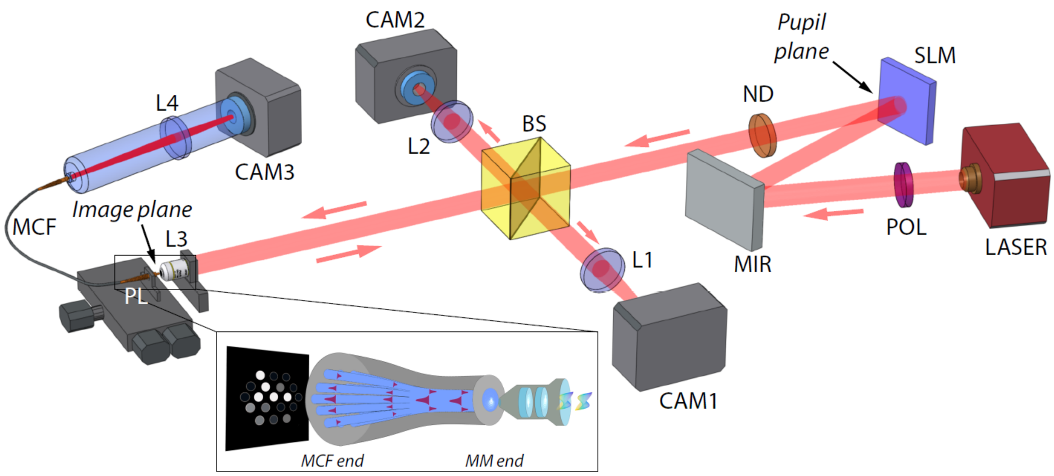

Fig.2. Diagram of the laboratory setup used for testing the photonic lantern wavefront sensor. A collimated 685 nm laser (LASER) is passed through a linear polariser (POL) and via a fold mirror (MIR) onto a spatial light modulator (SLM), with a neutral density filter (ND) used to attenuate the beam. A wavefront constructed from a chosen set of Zernike terms is created by the SLM and focused to an image and injected by a microscope objective (L3) into the multimode end of the photonic lantern (PL). The intensity of the 19 outputs is then transmitted via multicore fiber (MCF) measured by a camera (CAM3) via lens L2. The raw PSF is also imaged via beamsplitter BS and lens L1 onto camera CAM1. The back-reflection off the fiber tip is imaged via the same beamsplitter and separate imaging system (L2, CAM2) to aid with alignment.

The 19 output intensities from the photonic lantern were then recorded, and the images of the PSF and back-reflection from the fiber are also saved for reference. This was then repeated for the desired number of samples. For the results in this demonstration, a data set of approximately 60000 measurements was taken, which would take of order 30 seconds to acquire with a contemporary extreme AO system running at kHz speeds. Of these data, 20% were reserved as validation samples and the rest are used as training samples. To evaluate the performance of the network, the 19 output fluxes for previously unseen laboratory test data were given to the neural network and the wavefront coefficients predicted, and the mean-squared error between the predicted coefficients and the true coefficients calculated. The neural network was able to reconstruct the incident wavefront error to varying degrees of accuracy depending on the model architecture chosen. It was also found that a deep network (i.e. including hidden layers) was required for optimum performance. The best performing network with above (RMSE = $5.1\text{x}10^{-3}$ π) consisted of 3 layers arranged in a 'funnel' configuration, with each layer having 2000, 1050 and 100 units respectively.

4. Conclusion

The photonic lantern wavefront sensor (PL-WFS) represents a type of wavefront sensor which addresses several of the limitations of current adaptive optics systems. Placing the wavefront sensor at the focal plane, rather than at a non-common pupil plane, has been long desired in adaptive optics as it eliminates non-common path error and is sensitive to wavefront errors not visible in the pupil plane (such as island modes). Simulations validated the principle of the device, and laboratory demonstrations confirmed its operation. In laboratory tests, wavefront errors with P-V amplitude of π radians constructed using the first 9 (non-piston) Zernike terms are introduced, and are then accurately reconstructed from a focal plane measurement using the PL-WFS, to a precision of 5.1×10^{-3} π radians root-mean-squared-error.

5. References

[1] Leon-Saval et al., Nanophotonics 2 (5-6), 429-440 (2013).
[2] Birks et al, Adv. Opt. Photon., 7(2):107–167 (2015).
[18] Norris et al, Nat Commun 11, 5335 (2020).
[19] Cruz-Delgado et al, Opt. Lett. 46, 3292-3295 (2021).
[23] Corrigan et al, Adaptive Optics Systems VI, volume 10703, 1313 – 1320. International Society for Optics and Photonics, SPIE (2018).
[24] Lecun et al, Nature 521, 436–444 (2015).